Journal of Power Sources 193 (2009) 99–106

Contents lists available at ScienceDirect

Journal of Power Sources

journal homepage: www.elsevier.com/locate/jpowsour

# Kinetic study of the hydrogen oxidation reaction on sub-stoichiometric titanium oxide-supported platinum electrocatalyst in acid solution

B. Babić[a], J. Gulicovski[a], Lj. Gajić-Krstajić[b], N. Elezović[c], V.R. Radmilović[d], N.V. Krstajić[e,*], Lj.M. Vračar[e]

[a] Vinča Institute of Nuclear Sciences, P.O. Box 522, Belgrade, Serbia
[b] Institute of Technical Sciences-SASA, Belgrade, Serbia
[c] Center of Multidisciplinary Researches, Belgrade, Serbia
[d] National Center for Electron Microscopy, LBLN University of California, Berkeley, USA
[e] Faculty of Technology and Metallurgy, University of Belgrade, Belgrade, Serbia

ARTICLE INFO

*Article history:*
Received 10 October 2008
Received in revised form
26 November 2008
Accepted 26 November 2008
Available online 24 December 2008

*Keywords:*
Titanium sub-oxide
Hydrogen oxidation reaction
Kinetic equation
Mechanism

ABSTRACT

The kinetics and mechanism of the hydrogen oxidation reaction were studied in 0.5 mol dm$^{-3}$ $HClO_4$ solution on an electrode based on titanium oxide with Magneli phase structure-supported platinum electrocatalyst applied on rotation Au disk electrode. Pt catalyst was prepared by impregnation method from 2-propanol solution of $Pt(NH_3)_2(NO_2)_2$ and sub-stoichiometric titanium oxide powder. Sub-stiochiometric titanium oxide support was characterized by X-ray diffraction and BET techniques. The synthesized catalyst was analyzed by TEM technique. Based on Tafel–Heyrovsky–Volmer mechanism the corresponding kinetic equations were derived to describe the hydrogen oxidation current–potential behavior on RDE over the entire potential region. The polarization RDE curves were fitted with derived polarization equations according to proposed model. The fitting shows that the HOR on Pt proceeds most likely via the Tafel–Volmer (TV) pathway in the lower potential region, while the Heyrovsky–Volmer (HV) pathway is operative in the higher potential region. It is pointed out that Tafel equation that has been frequently used for the kinetics analysis in the HOR, can not reproduce the polarization curves measured with high mass-transport rates. Polarization measurements on RDE revealed that the Pt catalyst deposited on titanium suboxide support showed equal specific activity for the HOR compared to conventional carbon-supported Pt fuel cell catalyst.



## 1. Introduction

The hydrogen oxidation reaction (HOR) is a very important reaction occurring in some kinds of electrochemical sensors and fuel cells. In acid media the catalysis of the reaction is usually promoted by the platinum based catalysts dispersed as nanoparticles on carbon supports [1–3].

According to the literature data there are many questions that are still open with regard to the kinetics and mechanism of HOR, even at Pt in pure hydrogen. Still, there is no unique statement of the nature of the H intermediate. Kita and Gao [4] suggested that possible routes in the HOR mechanism on Pt single crystal electrode could be different from the routes in the hydrogen evolution reaction (HER), and that underpotentialy deposited hydrogen ($H_{upd}$) could be included in the oxidation reaction, too. Conway and Jerkiewicz [5] reported their results where direct respective parallels between underpotentialy and overpotentially deposited hydrogen ($H_{opd}$) discharge kinetics at various Pt surfaces where not found out, due to the different bonding situation of these species. They have stated that although the Volmer step in the HER is formally identical with $H_{upd}$ process it takes place on a surface that is already occupied by $H_{upd}$. Electrochemical measurements and spectroscopic analysis presented in the work of the Kunimatsu et al. [6] suggested direct interaction between $H_{upd}$ and $H_{opd}$ stressing that adsorbed H species, detected, were the intermediate of HOR and HER on Pt, and that is $H_{opd}$. Contrarily, Chen and Kucernak [7] demonstrated that $H_2$ adsorption process was the slow step during hydrogen oxidation, and that it was necessary to consider weakly and strongly adsorbed H with independent exchange current densities and interaction parameters. They stated that it was not useful to investigate the kinetics of the HOR at rotating disc electrode (RDE) because it exhibited completely diffusion controlled polarization behavior even when using an RDE at rotation rate up to 7000 rpm [8] and demonstrated that the single particle electrodes with sub-micrometer size provided very high mass transport rate, allowing the mechanism and kinetics of the HOR to be clearly revealed [7].

Chen and Kucernak [7] in the same paper emphasized that the contribution of the back reactions in the HOR could not be

* Corresponding author. Fax: +381 113370387.
*E-mail address:* nedeljko@tmf.bg.ac.yu (N.V. Krstajić).

0378-7753/$ – see front matter © 2008 Elsevier B.V. All rights reserved.
doi:10.1016/j.jpowsour.2008.11.142

ignored and therefore the kinetic current, $j_k$, that derived polarization behavior for the HOR should be expressed by the full Butler–Volmer equation, which means that polarization equation for the HOR cannot be simplified with linear Tafel equation. They confirmed, through the simulation of the experimental polarization data, that the HOR could be explained with the Tafel–Volmer (TV) reaction mechanism with the exchange current density of about 27 mA cm$^{-2}$, which is much higher than that measured by using RDE in acid solutions (~1 mA cm$^{-2}$). It is also quite interesting that the most frequently referred value of the exchange current density for the HOR which takes place through the same reaction path near the reversible potential at Pt in acid solution is also around 1 mA cm$^{-2}$ [9,10]. Based on published polarization data measured on single submicroparticles of Pt electrocatalyst [7] and Tafel–Volmer–Heyrovsky mechanism, Wang et al. [11] have developed a dual-pathway kinetic equation that describes HOR kinetics that fits these experimental data. They showed that reaction proceeded through the Tafel–Volmer pathway at lower overpotentials and through the Heyrovsky–Volmer (HV) pathway at $\eta > 50$ mV. Corresponded values of the exchange current densities obtained from the best fits of the microelectrode polarization curves are $j_{0T} \approx 470$ mA cm$^{-2}$ (Tafel step) and $j_{0H} \approx 10$ mA cm$^{-2}$ (Heyrovsky step).

The importance of the supporting material for the functioning of the catalysts is well recognized. It has to offer a highly developed surface combined with excellent electronic conductivity and corrosion resistance.

The main advantage of the carbon support is its extremely high surface area combined with excellent electro-conductivity. The ability to achieve a high dispersion and compositional homogeneity of the metal clusters on the support is another important requirement for an enhanced electrocatalytic activity, which is also fulfilled by carbon. Thus, carbon is currently the most widely used catalyst support. However, Kangasniemi et al. [12] have recently reported that the surface of Vulcan X-72 (Cabot), common carbon catalyst support material, is oxidized under conditions simulating the cathode environment of a polymer electrolyte fuel cell (PEFC). Moreover, it was found that Pt accelerated the corrosion rate of the carbon support [13,14]. Accordingly, corrosion of the cathode catalyst support may affect the durability of PEFC.

On the other hand, the anode catalyst could also be exposed to much more oxidative conditions than the cathode during the cell voltage reversal caused by fuel starvation [15]. In such a situation, the potential of the anode would exceed the $O_2$ evolution potential causing the oxidation of carbon support which may lead to significant irreversible deterioration of the cell performance. Therefore, a more oxidation-resistance catalyst support is preferable for a PEFC for the cathode and anode catalyst.

More recently other support catalysts have become available like a nonstoichiometric mixture of several titanium oxide phases, mainly $Ti_4O_7$ and $Ti_5O_9$, known as Magneli phases of the general formula $Ti_nO_{2n-1}$, where n is a number between 4 and 10. Commercially available product known as 'Ebonex' is supplied by Altraverda Ltd. (Sheffield, UK) [16–20]. Ebonex is electrochemically stable, with very high overpotentials for hydrogen and oxygen evolutions, in acid and base solutions, and high electrical conductivity of $10^3\ \Omega^{-1}\ cm^{-1}$, too [21], and that is why it could be suitable as catalyst support material. Since Ebonex is reduced titania and has hypo-d-electron character it is expected to have an ability to interact with inert noble metals, like platinum, changing additionally the catalytic activity of the platinum, according to the Brewer theory [22], or changing the adsorbate–surface interaction energy due to the move of the local d-bond position relative to the Fermi level, according to the Hammer and Norskov [23] concept.

The aim of this paper was to investigate the catalytic activity of Pt nanocatalyst, synthesized and dispersed on interactive home made $Ti_nO_{2n-1}$ support, using impregnation method towards HOR in acid media, and to develop kinetic equations for the HOR that could consequently describe kinetic behavior over the entire relevant potential region.

## 2. Experimental

### 2.1. Preparation and characterization of titanium oxide with Magneli phase structure

Magneli phases of general formula $Ti_nO_{2n-1}$, were synthesized in a typically synthesis that can be described as follows: 1.5 g of Ti acetyl-acetonate (Merck, Germany) was dissolved in 30 ml of absolute ethanol (Superlab, Serbia). The pH of the solution was adjusted to the value of 11 by dropwise adding of a certain amount of 1.0 mol dm$^{-3}$ $NH_4OH$ (~6 ml) under continuous stirring and then the sol was made. Prepared sol was infiltrated in 8 g of carbon cryogel, obtained using standard procedure [24], by pressure filtration technique. The filtration step was performed in laboratory set-up with a glass cylinder (allowing up to 10 bar air-pressure), and a system for air-supply and pressure regulation. The filtration process was typically performed at the constant pressure of 5 bar. After that, sol–gel process was occurred at room temperature for 48 h. The samples were dried by freeze-drying (Modulo Freeze Dryer System Edwards, England, consisting of freeze dryer unit with High Vacuum Pump E 2 M 8 Edwards). Each of samples were pre-frozen in deep-freeze refrigerator at −30 °C for 24 h. After that, they were frozen drying in the acrylic chambers with shelves arrangements mounted directly on the top of the condenser of Freeze Dryer. The vacuum during twenty hours of freeze-drying was around 4 mbar. Finally, for simultaneously removing of carbon and reduction of $TiO_2$, sample was placed in a conventional furnace, first in argon flow for 18 h, and than in air, for 4 h at 600 °C. After the treatment, the furnace was cooled at room temperature.

Adsorption and desorption isotherms of $N_2$ were measured on titanium oxide with Magneli phase structure at −196 °C, using the gravimetric McBain method [25]. The specific surface area, $S_{BET}$, and pore size distribution, were calculated from the isotherms. Pore size distribution was estimated by applying BJH method [26] to the desorption branch of isotherms. The morphology of the synthesized titanium oxide with Magneli phase structure was studied by scanning electron microscopy (SEM) using JEOL 6300F microscope.

### 2.2. Catalyst preparation

Pt catalyst was prepared by a conventional impregnation method using 2-propanol solution of $Pt(NH_3)_2(NO_2)_2$ (Merck) and titanium oxide powder with Magneli phase structure ($Ti_nO_{2n-1}$) as supporting material. The preparation process can be described as follows: Appropriate amount of $Pt(NH_3)_2(NO_2)_2$ solution (10 mg Pt ml$^{-1}$) was slowly added to 90 mg of support powder. This was ultrasonically blended for 1 h and after thorough mixing, the precursor suspension was allowed to dry at 80 °C for 12 h. The precursor powder was then set in a tube furnace and reduced under flowing $H_2$ gas at 300 °C for 2 h and cooled at room temperature under flowing inert (Ar) gas. The Pt loading of the all catalysts was always 10 wt.%.

### 2.3. Electrode preparation

Five milligram of $Ti_nO_{2n-1}$/Pt catalyst was ultrasonically suspended in 1.0 ml of water–methanol (v/v = 1/1) and 50 μl of Nafion solution (5 wt.% Aldrich solution) to prepare catalyst ink. Then, 10.0 μl of ink was transferred with an injector to the clean gold disk electrode (6 mm diameter, with geometric surface area of

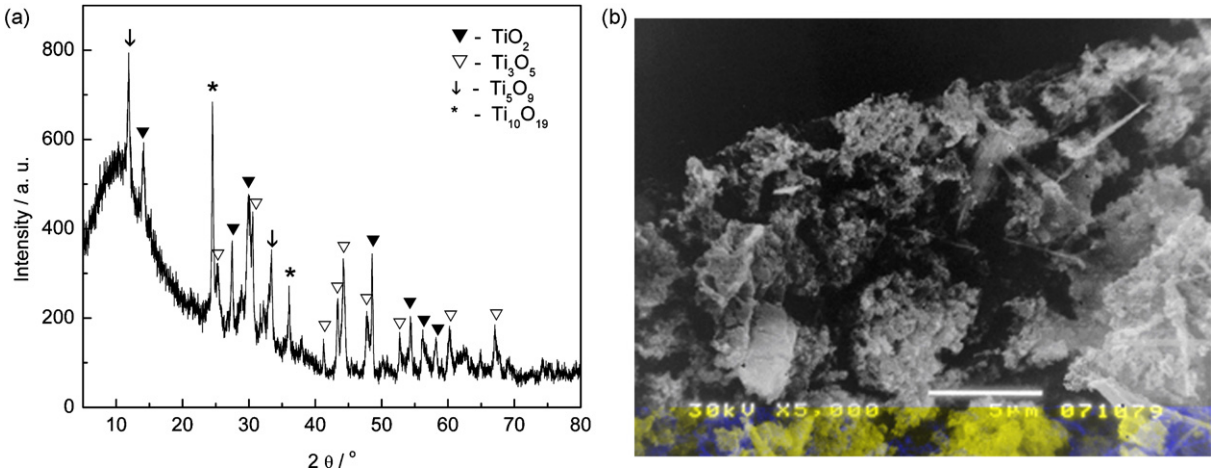


**Fig. 1.** (a) XRD pattern of titanium oxide with Magneli phase structure. (b) SEM image of titanium oxide with Magneli phase structure.

0.28 $cm^2$). After the water-methanol volatilization, the electrode was heated at 80 °C for 10 min. The Pt loading of the catalyst was always 5 μg.

### 2.4. Electrode characterization

Transmission electron microscopy (TEM) measurements were performed using the FEI (Fillips Electronic Instruments) – CM200 super-twin and CM300 ultra-twin microscopes operating at 200 and 300 kV and equipped with the Gatan 1k × 1k and 2k × 2k CCD cameras, respectively. Specimen was prepared for transmission electron microscopy by making suspension of the catalyst powder in ethanol, using an ultrasonic bath. This suspension was dropped onto clean holey carbon grids and was then dried in air.

### 2.5. Electrochemical characterization

A reversible hydrogen electrode (RHE) in the same solution as that of the working electrode was used as the reference electrode. A large-area platinum sheet of 5 $cm^2$ geometric area was used as the counter electrode. The electrochemical measurements were performed in 0.5 mol $dm^{-3}$ $HClO_4$ solution (Spectrograde, Merck), prepared in deionized water ("Millipore" – 18 MΩ), at the temperature of 25 °C.

The experiments were performed by potentiodynamic method. A PAR Model 273 Potentiostat/Galvanostat was used for all electrochemical experiments.

The cyclic voltammetry (CV) experiments were carried out in the potential range between hydrogen and oxygen evolution in 0.5 mol $dm^{-3}$ $HClO_4$ with various scan rates at a rotating speed of 2500 rpm.

## 3. 3.Results and discussion

### 3.1. Characterization of titanium oxide with Magneli phase structure

Fig. 1a shows the X-ray diffraction (XRD) pattern of Magneli phase sample, while the corresponding SEM image is presented in Fig. 1b. The diffraction peaks in the pattern can be indexed to $Ti_{10}O_{19}$, $Ti_5O_9$, $TiO_2$ (rutile) and $Ti_3O_5$ according to JCPDS card nos. 18-1405, 11-0193, 21-1276 and 8-0117. Titanium suboxides such as $Ti_{10}O_{19}$, $Ti_5O_9$ and $Ti_3O_5$ contain Ti atoms with the mixed valent states, Ti(III) and Ti(IV), which is the characteristic of titanium oxides with Magneli structure. The blue luster should result from the valence electron transition between Ti(III) and Ti(IV). The SEM image (Fig. 1b) shows that Magneli phase sample consists of the particles of agglomerates with uniformly sized spherical particles

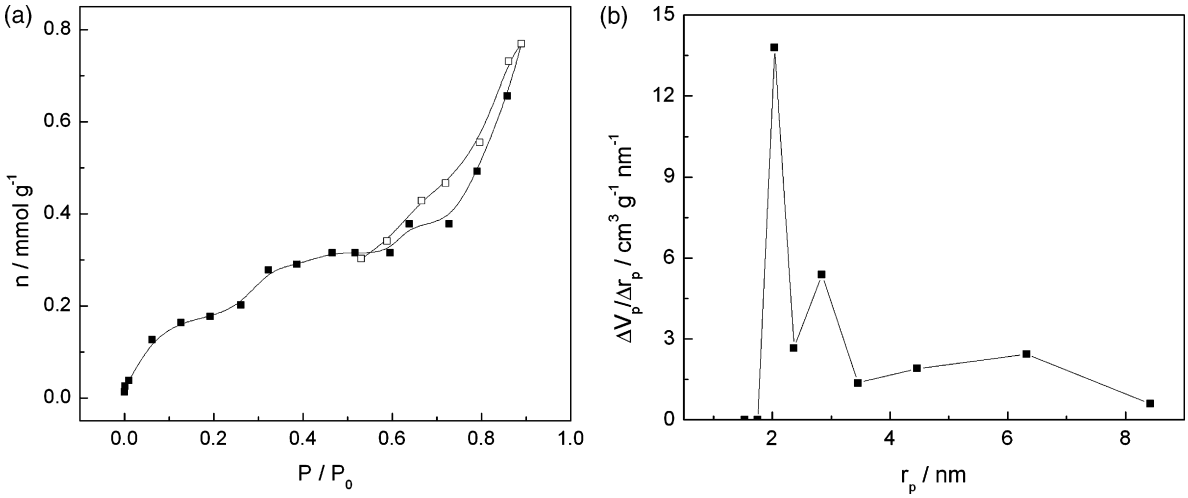


**Fig. 2.** (a) Nitrogen adsorption isotherms, as the amount of $N_2$ adsorbed as a function of relative pressure for titanium oxide support with Magneli phase structure. Solid symbols-adsorption, open symbols-desorption. (b) Pore size distribution of titanium oxide with Magneli phase structure.

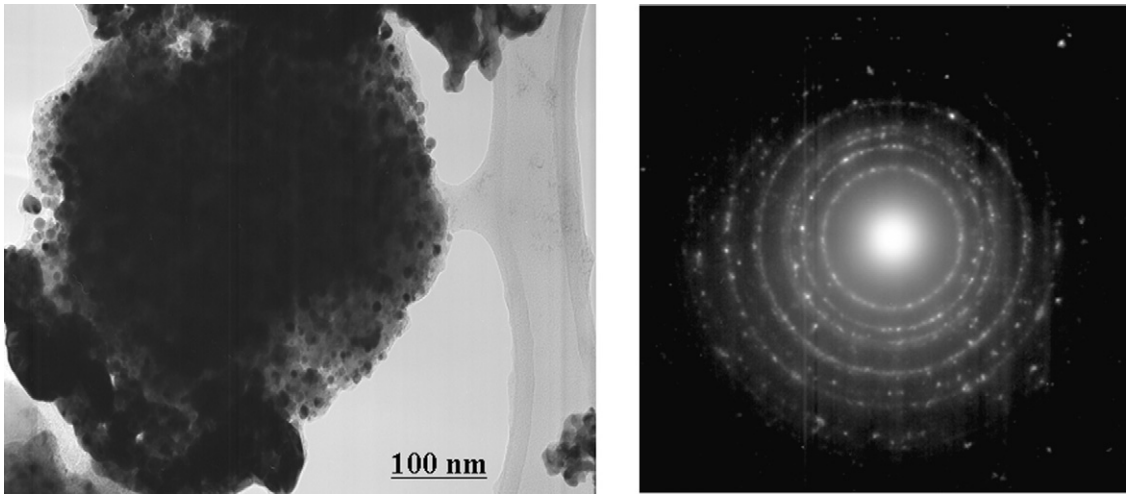


**Fig. 3.** TEM image of Pt nanoparticles on titanium oxide support with Magneli phase structure and the corresponding electron diffraction pattern of Pt nanoparticle.

inside the agglomerates whose distribution is rather wide, but with enough individual particles lower than few nm in size.

Nitrogen adsorption isotherms of titanium oxide with Magneli phase structure, as the amount of $N_2$ adsorbed as function of relative pressure at −196 °C, are shown in Fig. 2a. According to the IUPAC classification [27] isotherms are of type IV and with a hysteresis loop which is associated with mesoporous materials. Specific surface area calculated by BET equation, $S_{BET}$, is 15 $m^2\,g^{-1}$. Pore size distribution (PSD) of titanium oxide with Magneli phase structure ($Ti_nO_{2n-1}$) is shown in Fig. 2b. Figure shows that samples are mesoporous with most of the pores radius between 2 and 9 nm.

### 3.2. TEM analysis

Fig. 3 depicts a typical TEM image of in-house $Ti_nO_{2n-1}$/Pt catalyst. The Pt nanoparticles are globular in shape with a very wide size distribution. Some of the larger particles appear to be agglomerates of few smaller ones. However, it was not possible to determine accurately Pt particle size distribution and to calculate the total surface area of the Pt particles by analyzing different region of the catalyst from images, because of non-uniform distribution of the catalyst at $Ti_nO_{2n-1}$ support. The investigation of Pt nanoclusters by electron diffraction (right hand side of Fig. 3) shows that Pt nanoparticles are highly crystalline with *fcc* structure.

### 3.3. Cyclic voltammetry results

Cyclic voltammetry tests were performed in 0.5 mol $dm^{-3}$ $HClO_4$ (as shown in Fig. 4). The CV-curve of $Ti_nO_{2n-1}$/Pt (5 μg) represents typical voltammogram of Pt with very clear hydrogen adsorption-desorption and PtOH formation and reduction regions, with the well defined cathodic peak at 0.80 V (RHE), observed during the reduction potential scan that represents reduction of oxygen adsorbed species.

CV was performed to determine the electrochemical surface area and to elucidate the adsorption properties of the catalyst. The electrochemically active surface area of the catalyst was calculated from the charge associated with the anodic desorption peak of UPD hydrogen. The base line was taken by extrapolation of the double-layer region of the voltammogram. The electrochemically active surface area of the catalyst ($S_{easa}$) was calculated from the measured charges assuming 210 μC $cm^{-2}$ as a charge of full coverage. This calculation gives the value of 35 $m^2\,g^{-1}$ (Pt) that is quite high keeping in mind low specific area of $Ti_nO_{2n-1}$ support.

### 3.4. Kinetics of the hydrogen oxidation at $Ti_nO_{2n-1}$/Pt catalyst

#### 3.4.1. Theoretical considerations

The hydrogen oxidation reaction in acid media can be written as:

$$H_2 \rightarrow 2H^+ + 2e \quad (1)$$

The corresponding elementary steps for the Tafel–Heyrovsky–Volmer mechanism on Pt catalyst are:

$$H_2 + 2Pt \underset{k_{-T}}{\overset{k_T}{\Leftrightarrow}} 2H\text{–}Pt \quad \text{(Tafel reaction)} \quad (2)$$

$$H_2 + Pt \underset{k_{-H}}{\overset{k_H}{\Leftrightarrow}} H\text{–}Pt + H^+ + e \quad \text{(Heyrovsky reaction)} \quad (3)$$

$$H\text{–}Pt \underset{k_{-V}}{\overset{k_V}{\Leftrightarrow}} Pt + H^+ + e \quad \text{(Volmer reaction)} \quad (4)$$

In the Tafel–Volmer pathway the dissociative adsorption of hydrogen molecule is followed by two separate one-electron oxidations of adsorbed H atoms. However, in the Heyrovsky–Volmer pathway, one-electrooxidation occurs simultaneously with chemisorption, followed by another one-electron oxidation of the adsorbed H atom.

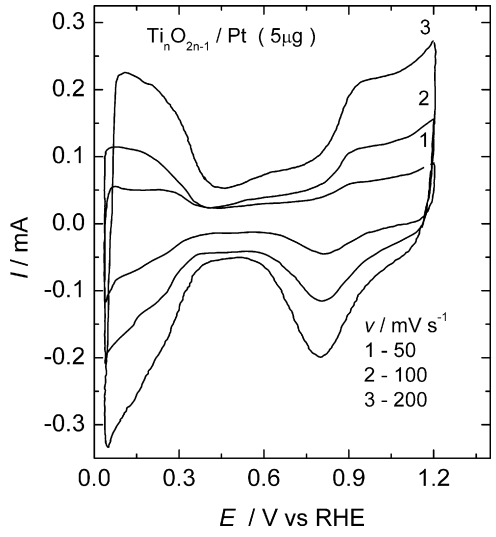


**Fig. 4.** Cyclic voltammograms for $Ti_nO_{2n-1}$/Pt (5 μg) electrode at different sweep rates, in $N_2$ saturated 0.5 mol $dm^{-3}$ $HClO_4$ solution at 25 °C.

In steady-state, the kinetics of the HOR for the simultaneous occurrence of the Tafel–Volmer and Heyrovsky–Volmer routes can be described on terms of the reaction rate of the elementary steps by following equation:

$$\upsilon F = I = 2F(\upsilon_T + \upsilon_H) = F(\upsilon_H + \upsilon_V) \tag{5}$$

where $\upsilon$ is the overall reaction rate and $\upsilon_S$ is the reaction rate of the step S. In steady-state condition, reaction intermediate does not change with time: $d\Theta/dt = 2\upsilon_T + \upsilon_H - \upsilon_V = 0$.

The rate of the elementary steps, when Langmuir-type adsorption is considered for the adsorbed hydrogen, in the absence of mass-transfer limitations, and assuming that the electron transfer coefficient is 1/2, can be written as:

$$\upsilon_T = k_T(1-\Theta_H)^2 c_{H_2} - k_{-T}\Theta_H^2 \tag{6}$$

$$\upsilon_H = k_H(1-\Theta_H)c_{H_2}\exp(FE/2RT) - k_{-H}\Theta_H c_{H^+}\exp(-FE/2RT) \tag{7}$$

$$\upsilon_V = k_V\Theta_H\exp(FE/2RT) - k_{-V}(1-\Theta_H)c_{H^+}\exp(-FE/2RT) \tag{8}$$

where $k_S$ are the rate constants for each elementary steps, $\Theta_H$ is the coverage of the reaction $H$ intermediate, $c_{H_2}$ and $c_{H^+}$ are the concentration of dissolved hydrogen molecules, and protons, respectively.

At the reversible potential, $E^0$, the overall reaction rate is zero, and forward and backward reaction rates are equal, for each elementary step. Therefore, the exchange reaction rate for the three elementary steps can be expressed as:

$$\upsilon_{0T} = k_T(1-\Theta_H^0)^2 c_{H_2}^0 = k_{-T}(\Theta_H^0)^2 \tag{9}$$

$$\upsilon_{0H} = k_H(1-\Theta_H^0)c_{H_2}^0\exp(FE^0/2RT) = k_{-H}\Theta_H^0 c_{H^+}^0\exp(-FE^0/2RT) \tag{10}$$

$$\upsilon_{0V} = k_V\Theta_H^0\exp(FE^0/2RT) = k_{-V}(1-\Theta_H^0)c_{H^+}^0\exp(-FE^0/2RT) \tag{11}$$

where, $\Theta_H^0$, $c_{H_2}^0$, and $c_{H^+}^0$ denote the coverage and concentrations at $E = E^0$.Dividing the Eqs. (6)–(8) by their respective exchange rates in Eqs. (9)–(11), leads to:

$$\upsilon_T = \upsilon_{0T}\left[\left(\frac{1-\Theta_H}{1-\Theta_H^0}\right)^2\left(\frac{c_{H_2}}{c_{H_2}^0}\right) - \left(\frac{\Theta_H}{\Theta_H^0}\right)^2\right] \tag{12}$$

$$\upsilon_H = \upsilon_{0H}\left[\left(\frac{1-\Theta_H}{1-\Theta_H^0}\right)\left(\frac{c_{H_2}}{c_{H_2}^0}\right)\exp(F\eta/2RT) - \left(\frac{c_{H^+}}{c_{H^+}^0}\right)\left(\frac{\Theta_H}{\Theta_H^0}\right)\exp(-F\eta/2RT)\right] \tag{13}$$

$$\upsilon_V = \upsilon_{0V}\left[\left(\frac{\Theta_H}{\Theta_H^0}\right)\exp(F\eta/2RT) - \left(\frac{c_{H^+}}{c_{H^+}^0}\right)\left(\frac{1-\Theta_H}{1-\Theta_H^0}\right)\times\exp(-F\eta/2RT)\right] \tag{14}$$

In these equations, the term $c_{H^+}/c_{E^+}^0 \approx 1$ in acid solution and it is essentially constant during the HOR. The concentration of dissolved $H_2$ at Pt surface varies with the current and the mass transport rate. The relation is commonly described by the equation $c_{H_2}/c_{H_2}^0 = \left(1-\frac{I}{I_L}\right)$, where $I_L$ is the $H_2$ diffusion limiting current at high potential when $c_{H_2}$ approaches zero. Thus, the Eqs. (12) and (13) can be modified by incorporating these relationships and combining them with the Eq. (5), yields:

$$I = 2F\upsilon_{0T}\left[\left(\frac{1-\Theta_H}{1-\Theta_H^0}\right)^2\left(1-\frac{I}{I_L}\right) - \left(\frac{\Theta_H}{\Theta_H^0}\right)^2\right] + 2F\upsilon_{0H}\left[\left(\frac{1-\Theta_H}{1-\Theta_H^0}\right)\left(1-\frac{I}{I_L}\right)\exp(F\eta/2RT) - \left(\frac{\Theta_H}{\Theta_H^0}\right)\exp(-F\eta/2RT)\right] \tag{15}$$

Multiplying by $2F$ both sides of Eqs. (9) and (10) one can correlate the exchange rates to the exchange currents:

$$2F\upsilon_{0T} = 2Fk_T(1-\Theta_H^0)^2 c_{H_2}^0 = I_{0T}(1-\Theta_H^0)^2 \tag{16}$$

$$2F\upsilon_{0H} = 2Fk_H(1-\Theta_H^0)c_{H_2}^0\exp(FE^0/2RT) = I_{0H}(1-\Theta_H^0) \tag{17}$$

Incorporating Eqs. (16) and (17) into Eq. (15), leads to:

$$I = I_{0T}\left[(1-\Theta_H)^2\left(1-\frac{I}{I_L}\right) - (1-\Theta_H^0)^2\left(\frac{\Theta_H}{\Theta_H^0}\right)^2\right] + I_{0H}\left[(1-\Theta_H)\left(1-\frac{I}{I_L}\right)\exp(F\eta/2RT) - (1-\Theta_H^0)\left(\frac{\Theta_H}{\Theta_H^0}\right)\times\exp(-F\eta/2RT)\right] \tag{18}$$

Dependence of $\Theta_H$ on $\eta$ (or $E$) can be obtained by solving the equation $d\Theta/dt = 2\upsilon_T + \upsilon_H - \upsilon_V = 0$ at steady-state. Wang et al. [11] found that simple expression can be used under the assumption that Volmer reaction rate is sufficiently larger than the Tafel and Heyrovsky reaction rates. For sufficiently small $\Theta_H^0$ and $\eta \geq 0$ follows:

$$\frac{\Theta_H}{\Theta_H^0} = \exp(-F\eta/\gamma RT) \tag{19}$$

where $\gamma$ is the potential range constant for the adsorption isotherm determined by the exchange rates for the three elemental reactions and also function of $\Theta_H^0$. Previously, simulations [28] showed that $\Theta_H^0$ ranging from 0.09 to $10^{-7}$. Incorporating Eq. (19) into Eq. (18) and letting $(1-\Theta_H)$ and $(1-\Theta_H^0)$ be unity, Eq. (18) can be presented in more simplified form:

$$I = I_{0T}\left[\left(1-\frac{I}{I_L}\right) - \exp(-2F\eta/\gamma RT)\right] + I_{0H}\left[\left(1-\frac{I}{I_L}\right)\exp(F\eta/2RT) - \exp(-F\eta/\gamma RT)\exp(-F\eta/2RT)\right] \tag{20}$$

This can be rearranged as:

$$I = \frac{I_{0T}(1-\exp(-2F\eta/\gamma RT) + I_{0H}[(\exp(F\eta/2RT) - \exp(-F\eta/\gamma RT)\exp(-F\eta/2RT)]}{1 + I_{0T}/I_L + I_{0H}/I_L\exp(F\eta/2RT)} = \frac{I_k}{1+I_f/I_L} \tag{21}$$

The numerator in the above equation corresponds to the kinetic current, $I_k$, when the limiting current, $I_L \to \infty$. The sum of the two positive terms in the dominator represents the kinetic current of the forwards reactions, $I_f$.

Here, $I_{0T}$, $I_{0H}$ and $\gamma$ are the three essential kinetic parameters.

Wang et al. [11] have shown that the HOR takes place dominantly through Tafel–Volmer pathaway on Pt for $\eta \leq 50$ mV, where the current rises rapidly in an inverse exponential function. In this case, Eq. (20) can be presented in a more simplified form:

$$I = I_{0T}\left[\left(1-\frac{I}{I_L}\right) - \exp(-2F\eta/\gamma RT)\right] \tag{22}$$

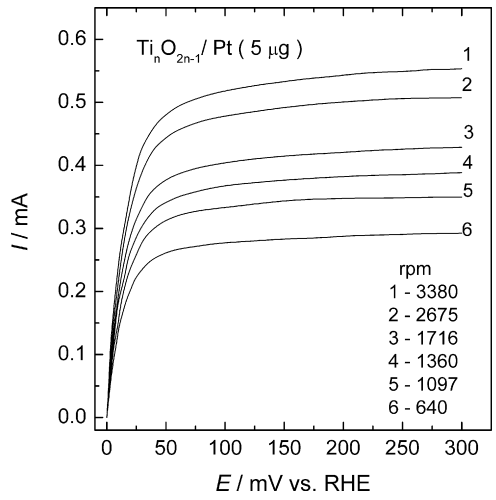


**Fig. 5.** Polarization curves obtained with rotating disk electrode at $v = 2$ mV s$^{-1}$ for $H_2$ oxidation in 0.5 mol dm$^{-3}$ $HClO_4$ solution at $Ti_nO_{2n-1}$/Pt, for several rotation speeds.

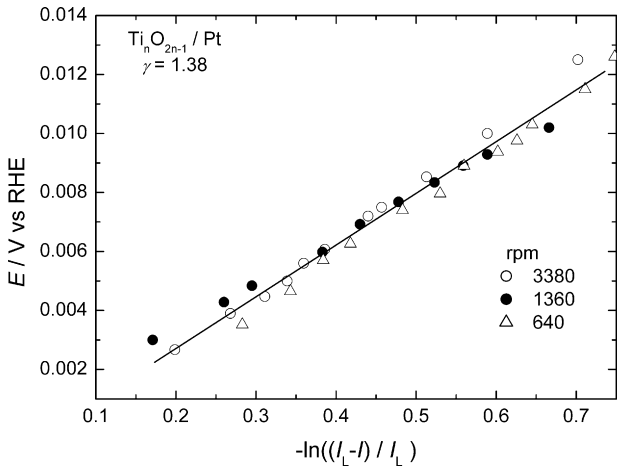


**Fig. 6.** Measured (symbols) and fitted (lines) polarization curves for the HOR on $Ti_nO_{2n-1}$/Pt RDE at different rotation rates in hydrogen saturated 0.5 mol dm$^{-3}$ $HClO_4$ solution at 25 °C. Fitted curves were obtained using Eq. (25) in order to determine the kinetic parameter $\gamma$.

and rearranged as:

$$I = \left(\frac{I_{0T} I_L}{I_{0T} + I_L}\right)[1 - \exp(-2F\eta/\gamma RT)] \quad (23)$$

or:

$$\exp(-2F\eta/\gamma RT) = 1 - \frac{I}{I_{0T}} - \frac{I}{I_L} \quad (24)$$

If the $I_{0T} \gg I$ condition is fulfilled (this condition can be easily fulfilled even in RDE measurements), than the second term on the right side of Eq. (24) can be neglected and equation becomes:

$$\eta = -\frac{\gamma RT}{2F} \ln\left(\frac{I_L - I}{I_L}\right) \quad (25)$$

Eq. (25) is the similar to the Nernstian equation $\left(E = -\frac{RT}{2F} \ln\left(\frac{I_L - I}{I_L}\right)\right)$ for pure diffusion controlled reaction when Tafel and Heyrovsky elemental steps are in the quasi-equilibrium state, and which is frequently used to prove that the HOR takes place as the reversible reaction.

### 3.4.2. Determination of the kinetic parameters

Fig. 5 presents the hydrogen oxidation polarization curves for several rotation speeds, obtained at scan rate of 2 mV s$^{-1}$. The current is increased rapidly with potential on each curve and reach limiting value at ca. 50 mV (RHE).

The HOR polarization curves presented in Fig. 5 were first analyzed in low potential region using Eq. (25) in order to calculate the kinetic parameter, $\gamma$. The solid lines in Fig. 6 show that agreement with the data is obtained for the value of $\gamma = 1.38$ which does not depend on the rotation rate. Assuming also, that HOR takes place dominantly through the Tafel–Volmer pathway in low potential region, and if, for instance $\eta \leq 5$ mV the overall reaction rate can be presented by Eq. (22) in which the exponential may be expanded and higher terms neglected, so that one obtains:

$$\frac{I}{\eta} = \frac{2F}{\gamma RT}\left(\frac{I_L I_{0T}}{I_{0T} + I_L}\right) \quad (26)$$

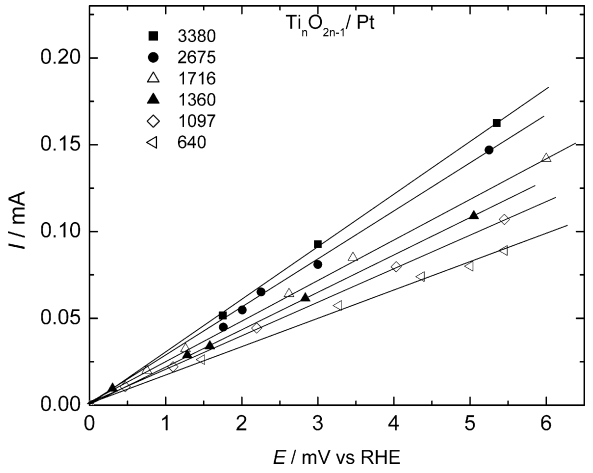


**Fig. 7.** Experimental data (symbols) and fitted (lines) polarization curves for the HOR on $Ti_nO_{2n-1}$/Pt RDE in hydrogen saturated 0.5 mol dm$^{-3}$ $HClO_4$ solution at 25 °C. Fitted curves were obtained using Eq. (26) and the kinetic parameter $\gamma = 1.38$, previously determined.

Fig. 7 presents the corresponding polarization data recorded at different rotation rates in low potential region. Values of exchange current for Tafel step, $I_{0T}$ were calculated from the slope of linear $\eta - I$ (or $E$ (RHE) $- I$), using Eq. (26), (mean value is presented in Table 1). Now, it is possible to estimate the last third kinetic parameter, $I_{0H}$ by fitting the RDE polarization curves in the whole potential range with Eq. (21). The solid lines in Fig. 8 show that agreement with the polarization data (symbols) is obtained by the best fits with one variable kinetic parameter. The values of the calculated kinetic parameters that fit the polarization RDE curves are presented in Table 1.

Finally, as shown in Fig. 9, the Tafel–Volmer pathway is responsible for the high HOR activity on Pt at $\eta < 50$ mV, where the current rises rapidly in an inverse exponential fashion to a value close to $I_{0T}$. Further increases are realized through Heyrovsky–Volmer path-

**Table 1**
Calculated kinetic parameters for the HOR at titanium sub-oxide supported Pt catalyst.

| $Ti_nO_{2n-1}$-support, $S$ (m$^2$ g$^{-1}$) | Pt catalyst | | $I_{0T}$ | | | $I_{0H}$ | | | $\gamma$ |
|---|---|---|---|---|---|---|---|---|---|
| | m$^2$ g$^{-1}$ | cm$^2$ (5 μg Pt) | mA | mA cm$^{-2}$ | A mg$_{Pt}^{-1}$ | mA | mA cm$^{-2}$ | A mg$_{Pt}^{-1}$ | |
| 15 | 35 | 1.75 | 50 | 28.6 | 10 | 3 | 1.7 | 0.6 | 1.38 |

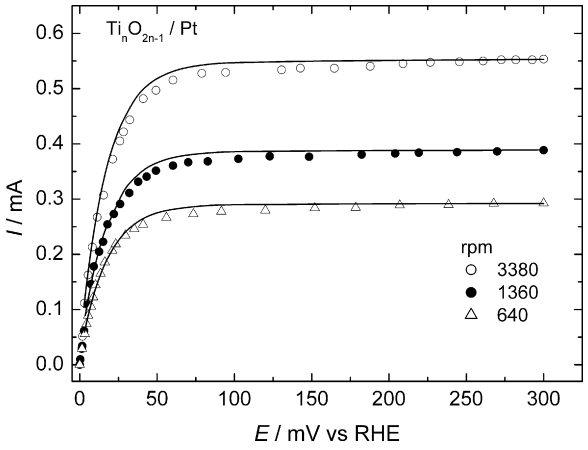


**Fig. 8.** Measured (symbols) and fitted (lines) polarization curves for the HOR on $Ti_nO_{2n-1}$/Pt RDE in hydrogen saturated 0.5 mol dm$^{-3}$ $HClO_4$ solution at 25 °C. Fitted curves were obtained using Eq. (21) and the corresponding kinetic parameters $\gamma = 1.38$ and $I_{0T} = 50$ mA, which had been previously determined.

way, which becomes important at high overpotentials where $I_{TV}$ levels off. For comparison, the kinetic current calculated using the Butler–Volmer equation $j_k = j_0(e^{2.3\eta/b} - e^{-2.3\eta/b})$ with $j_0 = 1$ mA cm$^{-2}$, and $b = 30$ mV dec$^{-1}$ was presented in Fig. 9, too (dotted-dashed line). The difference between the two kinetic curves is high and it is clear that Butler–Volmer equation cannot reproduce the polarization curves measured with high mass-transport rates as it was stated by Chen and Kucernak [7]. This conclusion that is based on our experimental results is in agreement with theoretical fact that if a preceding chemical adsorption is followed with electron transfer reaction, as we proposed in the kinetic analysis for HOR, then the using of Butler–Volmer equation could not be correct in performing the kinetic of the reaction.

Also, by comparing the feature of our curve in the low potential region (Fig. 9), that was calculated by using the proposed mechanism, with anodic polarization curve for the HOR, derived from half-cell under actual PEMFC operating conditions (29,30], one can see very good conformity.

Kinetic current, $I_k$, for the HOR at $E$ (RHE) = 30 mV is 45 mA (Fig. 9) which corresponds to the mass-specific current density of $j = 9$ A mg$_{Pt}^{-1}$. This finding shows that the Pt catalyst deposited on

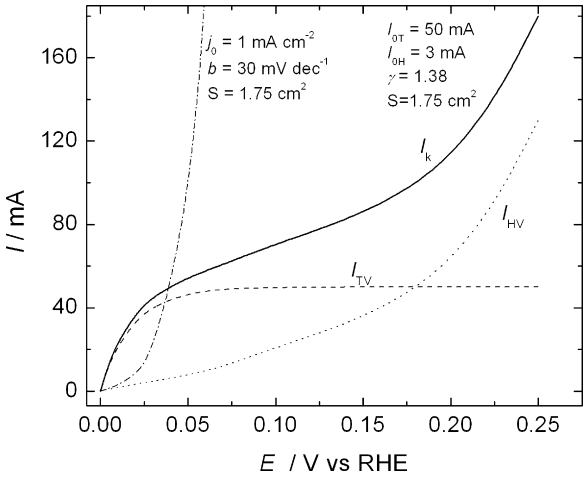


**Fig. 9.** Kinetic current for the HOR on $Ti_nO_{2n-1}$/Pt electrode at 25 °C calculated using the numerator in Eq. (21) with $I_{0T} = 50$ mA, $I_{0H} = 3$ mA and $\gamma = 1.38$. Dashed and dotted lines represent the contributions from the TV and HV pathways, respectively. Dashed-dotted line shows the kinetic currents calculated using the Butler–Volmer equation with $j_0 = 1$ mA cm$^{-2}$ and $b = 30$ mV dec$^{-1}$ and $S = 1.75$ cm$^2$.

titanium suboxide support exhibits similar specific activity for the HOR compared to a conventional carbon-supported Pt fuel cell catalyst in spite of the relatively low specific surface area of Pt catalyst (35 m$^2$ g$^{-1}$).

## 4. Conclusions

The kinetics and mechanism of electrochemical hydrogen oxidation reaction on home-made $Ti_nO_{2n-1}$/Pt electrode in a perchloric acid solution has been studied. Based on Tafel-Heyrovsky-Volmer mechanism the corresponding kinetic equations were derived to describe the HOR current behavior on RDE over the entire overpotential region. Appling these in analysis of the polarization curves measured for $Ti_nO_{2n-1}$/Pt (5 μg) at RDE three essential kinetic parameters were determined:

$I_{0T} = 50$ mA (10 A mg$_{Pt}^{-1}$), $I_{0H} = 3$ mA (0.6 A mg$_{Pt}^{-1}$) and $\gamma = 1.38$. It is pointed out that Tafel equation that has been frequently used for the kinetics analysis in the HOR cannot reproduce the polarization curves measured with high mass-transport rates. The fitting shows that the HOR on Pt proceeds most likely via the Tafel–Volmer pathway in the lower potential region, while the Heyrovsky–Volmer pathway is operative in the higher potential region. The Pt catalyst deposited on titanium suboxide support exhibits similar specific activity for the HOR compared to a conventional carbon-supported Pt fuel cell catalyst in spite of the relatively low specific surface area of Pt catalyst (35 m$^2$ g$^{-1}$).

The aim of our further work should be the improvement of the preparation procedure in order to increase the surface area of titanium sub-oxide support as a way of improving active surface area of the catalyst.

## Acknowledgment

This work is financially supported by the Ministry of Science and Technological Development, Republic of Serbia, under contact no. 142038. V. Radmilović acknowledges support by the US Department of Energy under contract #DE-AC02-05CH11231.

## References

[1] H. Uchida, K. Izumi, M. Watanabe, J. Phys. Chem. B 110 (2006) 21924–21930.
[2] M. Watanabe, Y. Zhu, H. Uchida, J. Phys. Chem. B 104 (2000) 1762–1768.
[3] H.A. Gasteiger, N. Marković, P.N. Ross, J. Phys. Chem. 99 (1995) 16757–16767.
[4] H. Kita, S. Ye, Y. Gao, J. Electroanal. Chem. 334 (1992) 351–357.
[5] B.E. Conway, G. Jerkiewicz, Electrochim. Acta 45 (2000) 4075–4083.
[6] K. Kunimatsu, H. Uchida, M. Osawa, M. Watanabe, J. Electroanal. Chem. 587 (2006) 299–307.
[7] S. Chen, A. Kucernak, J. Phys. Chem. B 108 (2004) 13984–13994.
[8] J. Harrison, Z. Khan, J. Electroanal. Chem. 30 (1971) 327–330.
[9] J.K. Norskov, T. Bligaard, A. Logadottir, J.R. Kitchin, J.G. Chen, S. Pandelov, U. Stimming, J. Eelectrochem. Soc. 152 (2005) J23–J26.
[10] S. Trasatti, J. Electroanal. Chem. 39 (1972) 163–184.
[11] J.X. Wang, T.E. Springer, R.R. Adžić, J. Electrochem. Soc. 153 (2006) A1732–A1740.
[12] K.H. Kangasniemi, D.A. Condit, T.D. Jarvi, J. Electrochem. Soc. 151 (2004) E125–E132.
[13] L.M. Roen, C.H. Paik, T.D. Jarvi, Electrochem. Solid-State Lett. 7 (2004) A19–A22.
[14] R. Makharia, P. Yu, J. Pisco, S. Koscha, H. Gasteiger, Meeting Abstract of 2004 Joint International Meetings (MA2004-02), 3–8 October, 2004.
[15] A. Tanigichi, T. Akita, K. Yasuda, Y. Miyazaki, J. Power Sources 130 (2004) 42–49.
[16] V. Jalan, E.J. Taylor, J. Electrochem. Soc. 130 (1983) 2299–2302.
[17] M. Marezio, P.D. Dernier, J. Solid State Chem. 3 (1971) 340–348.
[18] G.R. Dieckmann, S.H. Langer, Electrchim. Acta 44 (1998) 437–444.
[19] L. He, H.F. Franzen, J.E. Vitt, D.C. Johnson, J. Appl. Electrochem. 26 (1996) 785–793.
[20] E.E. Ferndon, D. Plecher, Electrchim. Acta 42 (1997) 1281–1285.
[21] R.F. Bartholomew, D.R. Frankl, Phys. Rev. 187 (1969) 828–833.
[22] L. Brewer, P.R. Wengert, Metall. Trans. 4 (1973) 83–104.
[23] B. Hammer, J.K. Norskov, Adv. Catal. 45 (2000) 71–129.
[24] B. Babić, B. Kaluđerović, Lj. Vračar, N. Krstajić, Carbon 42 (2004) 2617–2624.

[25] J.W. McBain, A.M. Bakr, J. Am. Chem. Soc. 48 (1926) 690–695.
[26] E.P. Barret, L.G. Joyner, P.P. Halenda, J. Am. Chem. Soc. 73 (1951) 373–380.
[27] K.S.W. Sing, D.H. Everett, R.A.W. Haul, L. Moscou, R.A. Pierotti, J. Rouquerol, et al., Pure Appl. Chem. 57 (1985) 603–619.
[28] M.R. Gennero de Chialvo, A.C. Chialvo, J. Electrochem. Soc. 147 (2000) 1619–1622.
[29] G.A. Camara, E.A. Ticianelli, S. Mukerjee, S.J. Lee, J. McBreen, J. Electrochem. Soc. 149 (2002) A748–A753.
[30] R.C. Jiang, H.R. Kunz, J.M. Fenton, J. Electrochem. Soc. 152 (2005) A1329–A1340.